Rate limiting step in ammonia synthesis using low-pressure nitrogen-hydrogen mixture plasma

Shogo Uebayashi and Koichi Sasaki*

Division of Applied Quantum Science and Engineering, Hokkaido University, Kita 13, Nishi 8, Kita-ku, Sapporo 060-8628, Japan

The contributions of atomic nitrogen, atomic hydrogen, and vibrational excited molecular nitrogen were compared in the synthesis of ammonia using low-pressure nitrogen-hydrogen mixture plasma. No specific catalysts were employed, and ammonia was synthesized via reactions on the surface of a stainless-steel chamber. It was found that the number of nitrogen atoms transported to the chamber wall per unit time approximately coincided with the synthesis rate of ammonia. On the other hand, the synthesis rate of ammonia was saturated with the number of transported hydrogen atoms. In addition, we observed no correlation between the synthesis rate of ammonia and the number of vibrational excited nitrogen molecules. The experimental results indicate that the adsorption of atomic nitrogen is the rate limiting step in the synthesis process of ammonia in the present experimental condition, where the flux of atomic nitrogen was 10^3 times lower than the flux of vibrational excited molecular nitrogen.

1. Introduction

Since ammonia attracts much attention as an energy carrier recently,[1,2] we must be prepared to satisfy the growth of the social demand for the production of ammonia. At the moment, the industrial production of ammonia is based on the Haber-Bosch method exclusively.[3,4] The Haber-Bosch method is understood to be economical, but the economical production cost of ammonia by the Haber-Bosch method is owing to the mass production which needs plant-level equipment.[5] However, some industrial fields require alternative production method that is suitable to the power grid with small-scale renewable energy sources.[6] We believe that plasma-assisted synthesis is a candidate for the small-scale production method of ammonia,[7–9] even if it is inferior to the Haber-Bosch method in terms of the production cost.

The Haber-Bosch method is a reaction process using iron-based catalysts at the thermodynamic equilibrium using nitrogen-hydrogen mixture. The rate limiting step in the Haber-Bosch method is dissociative adsorption of molecular nitrogen.[10] A high catalyst temperature

*E-mail: sasaki@qe.eng.hokudai.ac.jp

is necessary in the Haber-Bosch method since molecular nitrogen should overcome the high activation energy for dissociative adsorption, even though the production of ammonia from the mixture of nitrogen and hydrogen is an exoergic reaction. An advantage of the plasma-assisted synthesis of ammonia is the possibility of the low-temperature synthesis, since active species produced in nonequilibrium plasma by electron impact have higher adsorption probabilities than ground-state molecular nitrogen at low temperatures. The active species which may contribute to the low-temperature synthesis of ammonia are atomic nitrogen, atomic hydrogen, and molecular nitrogen at vibrational excited states. However, the experimental works that compare the contributions of the three active species quantitatively are limited to date.[11,12] even though this is the principal issue to understand the basic mechanism of plasma-assisted catalytic synthesis of ammonia.

Although we worked on the above issue using an atmospheric-pressure plasma in a previous work,[13] we used a low-pressure plasma source in the present work to realize a largely different composition of the three active species. We employed a miniature electron cyclotron resonance (ECR) plasma source. The reason for choosing the miniature ECR plasma source was its compatibility with an x-ray photoelectron spectroscopy system that is capable of the vacuum transfer of catalyst samples. We will examine the surface adsorption probabilities of plasma-activated nitrogen and hydrogen using the x-ray photoelectron spectroscopy system with the vacuum transfer of catalyst samples, and the results will be reported elsewhere. In the present work, we compared the synthesis rate of ammonia with the fluxes of atomic nitrogen, atomic hydrogen, and molecular nitrogen at vibrational excited states. The fluxes of the active species were evaluated from their densities which were measured by vacuum ultraviolet absorption spectroscopy (VUVAS) and threshold ionization mass spectrometry. On the basis of the correlation between the fluxes and the synthesis rate, we judged the most important species in catalytic synthesis of ammonia using low-pressure nitrogen-hydrogen plasma.

2. Experimental methods

2.1 Plasma source

The experimental apparatus is shown in Fig. 1 schematically. We employed a miniature ECR plasma source with a permanent magnet (SAIREM Aura-Wave) in this experiment. The plasma source was inserted into a stainless-steel tube with an inner diameter of 3.8 cm from the top, and the tube with the plasma source was welded to another stainless-steel tube which was arranged horizontally. The horizontal tube also had a diameter of 3.8 cm, and we observed a plasma with the optical emission in the region below the plasma source. No spe-

cific catalysts were employed in this experiment, and we expected the synthesis of ammonia via reactions on the surface of the stainless-steel vacuum chamber. Note that the gas-phase production of ammonia is not expected in the present experimental condition, since the rates of three-body reactions are negligible at the low pressure. The vacuum chamber was evacuated using a turbomolecular pump below 1×10^{-4} Pa. After the evacuation, the mixture of nitrogen and hydrogen, whose flow rates were controlled using mass flow controllers, was introduced into the vacuum chamber. The plasma source was connected to a microwave power supply at 2.45 GHz using a coaxial cable via a three-stab tuner for the impedance matching. The maximum microwave power was 100 W. When we measured the temporal variations of the densities of atomic nitrogen and atomic hydrogen in the afterglow, we applied pulsed microwave power to the miniature ECR plasma source. The temperature of the stainless-steel tubes was not controlled, but the temperature of the horizontal stainless-steel tube, which worked for the ammonia synthesis mainly, was close to the room temperature.

2.2 Density measurements of atomic nitrogen and atomic hydrogen

The horizontal stainless-steel tube had two ports on the side, and they were connected to another ECR plasma source and a vacuum ultraviolet (VUV) monochromator, as shown in Fig. 1(a). The second ECR plasma was used as the light source for VUVAS.[14,15] The light source plasma was ignited by applying a microwave power of 50 W to a Lisitano coil which was attached around a quartz tube. The magnetic field which was necessary for the ECR discharge was obtained by applying a dc current to a set of Helmholtz coil. The densities of atomic nitrogen and atomic hydrogen were determined based on the magnitudes of optical absorption at the resonant lines of atomic nitrogen ($^4S^o - ^4P$ transition at 120.0 nm) and atomic hydrogen ($^2S - ^2P^o$ transition at 121.6 nm). For measuring the atomic nitrogen density, the light source plasma was produced using pure nitrogen at a pressure of 0.2 mTorr, whereas the mixture of hydrogen and argon was used for measuring the density of atomic hydrogen. The partial pressures of hydrogen and argon were 0.1 and 0.9 mTorr, respectively. The low pressures of nitrogen and hydrogen were necessary to avoid the measurement error caused by the spectral distortion of the resonant lines due to radiation trapping in the light source plasma.[16] The resonant line emissions transmitted through the region below the miniature ECR plasma source were discriminated using the VUV monochromator, and they were detected using a secondary electron multiplier (SEM) tube. The light source plasma, the miniature ECR plasma, and the VUV monochromator were separated by two MgF_2 windows. The electrical signal from SEM was recorded using a digital oscilloscope with an input

impedance of 1 MΩ. When we measured the temporal variations of the densities of atomic nitrogen and atomic hydrogen with a high temporal resolution in the afterglow phase of a pulsed discharge of the miniature ECR plasma, we used a multichannel scaler with an input impedance of 50 Ω to record the electrical signal from SEM. In this case, the intensities of the resonant line emissions transmitted through the miniature ECR plasma were recorded at the photon counting mode, where we recorded the relative number of photons arrived at SEM as a function of the delay time after the termination of the pulsed discharge.

2.3 Density measurement of molecular nitrogen at vibrational excited states

The density of molecular nitrogen at vibrational excited states was measured by threshold ionization mass spectrometry. This method is equivalent to molecular beam mass spectrometry reported by Jiang *et al.*,[17] and the principles and the performance of our system have been reported elsewhere.[18] Briefly, an orifice with a diameter of 0.5 mm was attached on a side port, as shown in Fig. 1(b), and the gas in the plasma with optical emission was sampled into another chamber equipped with a quadrupole mass spectrometer (QMS, Hiden Analytical HAL201). The QMS chamber was differentially evacuated using a turbomolecular pump. Unlike the previous paper,[18] the QMS head was inserted from the perpendicular direction to the line passing through the miniature ECR plasma and the orifice, as shown in Fig. 1(b). This configuration was intended to avoid the transport of positive ions in the plasma to QMS, which was the dominant noise source in this measurement. Considering a destruction probability on the order of 10^{-4} on the stainless-steel surface,[19] we expected the transport of molecular nitrogen at vibrational excited states to QMS via the scattering on the surface of the QMS chamber. We measured the QMS signal at $m/z = 28$ (molecular nitrogen ion) as a function of the electron beam energy in QMS. This signal was called the threshold ionization curve. The threshold ionization curve essentially represented the cross section of electron impact ionization of molecular nitrogen if the miniature ECR plasma was switched off, even though it was distorted by the finite broadening of the electron beam energy. We observed the enhancement in the QMS signal at electron energies lower than the ionization potential of molecular nitrogen if it was sampled from the plasma, which was attributed to ionization of molecular nitrogen at vibrational excited states. The vibrational temperature of molecular nitrogen was estimated by analyzing the low-energy part of the threshold ionization curve, and the density of vibrational excited molecular nitrogen ($v \geq 1$) was obtained from the vibrational temperature.

2.4 Measurement of synthesis rate of ammonia

If we adjust QMS at $m/z = 17$, the QMS signal tells us the relative density of ammonia in the plasma chamber. However, we cannot measure the synthesis rate of ammonia just by measuring the QMS signal at $m/z = 17$, since the density is determined by the balance between the synthesis rate and the destruction frequency of ammonia in the plasma. To estimate the synthesis rate of ammonia separately, we adopted the calibration method reported elsewhere.[20)] Briefly, we added a small amount of ammonia into the plasma chamber for the calibration. We observed a linear relationship if we plotted the QMS signal at $m/z = 17$ as a function of the flow rate of ammonia. The synthesis rate and the destruction frequency of ammonia were estimated from the intercept on the horizontal axis and the slope of the linear relationship, respectively. Note that the measurement of the synthesis rate was performed simultaneously with the density measurements of atomic nitrogen, atomic hydrogen, and molecular nitrogen at vibrational excited states. This was because the simultaneous measurement was important to obtain the accurate correlation between the synthesis rate and the fluxes of the active species, since the reproducibility of the measurement results was insufficient in the present experimental configuration, where the ratio of the volume to the surface area of the plasma chamber was smaller than usual plasma experiments. When we measured the densities of atomic nitrogen and atomic hydrogen by VUVAS, another QMS installed in a differentially evacuated chamber was used for the measurement of the synthesis rate, as shown in Fig. 1(a). When we measured the density of molecular nitrogen at vibrational excited states, the same QMS as that used for the threshold ionization mass spectrometry was used for the measurement of the synthesis rate.

3. Results and Discussion

3.1 Lifetimes of atomic nitrogen and atomic hydrogen

VUVAS tells us the line-integrated densities of atomic nitrogen and atomic hydrogen along the pass of the probe light or the axial direction of the horizontal stainless-steel tube. The densities of atomic nitrogen and atomic hydrogen can be estimated by dividing the line-integrated densities by the absorption lengths, which represent the lengths of the regions with atomic nitrogen and atomic hydrogen. To estimate the absorption lengths, we measured the temporal variations of the line-integrated densities of atomic nitrogen and atomic hydrogen in the afterglow phases of pulsed discharges.

Figure 2 shows the temporal variation of the line-integrated density of atomic nitrogen. The instantaneous microwave power to ignite the miniature ECR plasma was 50 W, and it was

pulse modulated at a repetition frequency of 100 Hz. The duration of the microwave power was 8 ms. The origin of the horizontal axis in Fig. 2 corresponds to the termination of the microwave power. The total gas pressure was 3.5 Pa, and the partial pressure ratio of nitrogen and hydrogen was $P_{N2}/P_{H2} = 1/3$. The system with the multichannel scaler for the photon counting measurement was employed to realize a high temporal resolution. Although the signal was rather noisy in the photon counting measurement, as shown in Fig. 2, we observed an exponential decrease in the line-integrated density of atomic nitrogen after the termination of the microwave power. The time constant of the exponential decrease was approximately $\tau_N = 0.3$ ms.

The temporal variation of the line-integrated density of atomic hydrogen is shown in Fig. 3. The instantaneous microwave power to ignite the miniature ECR plasma was 80 W, and it was pulse modulated at a repetition frequency of 0.2 Hz. The duration of the microwave power was 1 s. The total gas pressure was 3.5 Pa, and the partial pressure ratio of nitrogen and hydrogen was $P_{N2}/P_{H2} = 1/3$. As shown in Fig. 3(a), the lifetime of atomic hydrogen in the afterglow was much longer than that of atomic nitrogen, and it was approximately $\tau'_H = 1.1$ s. This lifetime was equivalent to the evacuation speed, indicating that the reactivity of atomic hydrogen in the afterglow was negligible. However, we also observed a sudden decrease in the atomic hydrogen density immediately after the termination of the microwave power, as shown Fig. 3(a). Since Fig. 3(a) was obtained by recording the probe light intensity using an oscilloscope, the temporal resolution was insufficient to analyze the sudden decrease. Hence, we switched the measurement system to the photon counting mode, and we repeated the measurement with a high temporal resolution, as shown in Fig. 3(b). The frequency of the pulse modulation and the duration of the microwave power were 100 Hz and 7 ms, respectively. Although the signal-to-noise ratio in the photon counting measurement was problematic, the lifetime of atomic hydrogen in the initial afterglow was roughly $\tau_H = 0.3$ ms, as shown in Fig. 3(b).

3.2 Estimation of surface loss probability and absorption length

Since the length of the horizontal stainless-steel tube is much longer than its radius, the decay time constant of the atomic nitrogen density is determined by[21)]

$$\tau_N = \frac{a^2}{5.78 D_N} + \frac{a(2-\alpha_N)}{\bar{v}_N \alpha_N}, \tag{1}$$

where D_N is the diffusion coefficient, a is the radius of the horizontal stainless-steel tube ($a = 1.9$ cm), α_N is the surface loss probability of atomic nitrogen, and $\bar{v}_N = \sqrt{8kT/\pi m_N}$ with k, T, m_N being the Boltzmann constant, the gas temperature, and the mass of atomic nitrogen,

respectively. The diffusion coefficient of atomic nitrogen in N_2 is reported in literature, and it is 2.46×10^2 cm^2/s at 1 Torr.[22,23] However, unfortunately we cannot find literature that reports the diffusion coefficient in H_2. Hence, we are forced to estimate 4×10^2 cm^2/s for the diffusion coefficient of atomic nitrogen in H_2 at 1 Torr by referring to the ratio between the diffusion coefficients of atomic hydrogen in N_2 and H_2.[24] Under this estimation, the diffusion coefficient of atomic nitrogen amounts to be $D_N = 2 \times 10^4$ cm^2/s in the nitrogen-hydrogen mixture in the present experimental condition (the total pressure of 3.5 Pa with $P_{N2}/P_{H2} = 1/3$). In this case, $\alpha_N \sim 0.2$ is estimated from $\tau_N = 0.3$ ms by assuming $T = 400$ K. This surface loss probability is consistent with literature values.[25–29] On the other hand, the transport length of atomic nitrogen along the axial direction of the horizontal stainless-steel tube is estimated to be $\sqrt{D_N \tau_N} \sim 2.6$ cm, if we assume $\tau_N = 0.3$ ms for the lifetime of atomic nitrogen in the discharge phase. Since the transport length of 2.6 cm is expected for atomic nitrogen in both the sides of the plasma, we assumed $L_N = 9$ cm for the absorption length in VUVAS.

The experimental result shown in Fig. 3 gives us an important insight into the kinetics of atomic hydrogen. The lifetime of $\tau_H = 0.3$ ms for atomic hydrogen in the initial afterglow is the same as the lifetime of atomic nitrogen. This means atomic hydrogen is rather reactive if atomic nitrogen is available. After the disappearance of atomic nitrogen, the reactivity of atomic hydrogen decreases remarkably. The surface of the stainless-steel tube may be passivated by adsorption of atomic hydrogen, resulting in a long lifetime of $\tau'_H = 1.1$ s. Since the diffusion coefficients of atomic hydrogen in H_2 and N_2 at 1 Torr are reported to be 1.6×10^3 and 9.9×10^2 cm^2/s, respectively,[24] the diffusion coefficient in the nitrogen-hydrogen mixture in the present experimental condition is estimated to be $D_H = 9.1 \times 10^4$ cm^2/s. By adopting the same equation as Eq. (1) to atomic hydrogen, the surface loss probability of atomic hydrogen is estimated to be $\alpha_H \sim 0.04$ from $\tau_H = 0.3$ ms. On the other hand, the transport length of atomic hydrogen along the axial direction of the horizontal stainless-steel tube is estimated to be $\sqrt{D_H \tau_H} \sim 5.2$ cm, if we assume $\tau_H = 0.3$ ms for the lifetime of atomic hydrogen in the discharge phase. Since the transport length of 5.2 cm is expected for atomic hydrogen in both the sides of the plasma, we assumed $L_H = 14$ cm for the absorption length in VUVAS.

3.3 Correlation between fluxes of active species and synthesis rate of ammonia

We carried out the measurements of the atomic nitrogen density n_N, the atomic hydrogen density n_H, the density of molecular nitrogen at vibrational excited states $n_{N_2(v)}$, and the synthesis rate of ammonia S_{NH_3} at various discharge conditions. The microwave power was var-

ied between 40 and 80 W. The total gas pressures were 1.5 − 10 Pa with the mixture ratios P_{N2}/P_{H2} between 3/1 and 1/3. As a result, we observed $1.1 \times 10^{17} \leq n_N \leq 3.2 \times 10^{17}$ m^{-3}, $1.2 \times 10^{17} \leq n_H \leq 4.6 \times 10^{17}$ m^{-3}, and $3.1 \times 10^{20} \leq n_{N_2(v)} \leq 5.1 \times 10^{21}$ m^{-3}. The synthesis rates of ammonia were $S_{NH_3} = (1 - 7) \times 10^{17}$ s^{-1}.

Since the gas-phase production of ammonia is not expected at the low pressure in the present experiment, the important parameters are the fluxes of active species toward the surface of the vacuum chamber. Figure 4 shows the correlation between the synthesis rate of ammonia and the integrated flux of atomic nitrogen. The integrated flux of atomic nitrogen was estimated by $\Gamma_N A_N$ with Γ_N and A_N being the thermal flux of atomic nitrogen and the effective surface area of the horizontal stainless-steel tube, respectively. The thermal flux was obtained by $\Gamma_N = 0.25 n_N \bar{v}_N$. The effective surface area was estimated by $A_N = 2\pi a L_N$, where $L_N = 9$ cm was assumed to be equal to the absorption length of atomic nitrogen. Although $L_N = 9$ cm is estimated by the lifetime measurement at 3.5 Pa, the value of $\Gamma_N A_N$ is not affected by L_N so much. This is because the raw data of VUVAS is the line-integrated density. n_N is inversely proportional to L_N, whereas A_N is proportional to L_N. n_N and A_N cancel each other out in the evaluation of the integrated flux $A_N L_N$, even if L_N is longer (or shorter) at a lower (or higher) pressure because of a higher (or lower) diffusion coefficient. The horizontal error bars in Fig. 4 represent the ambiguity in the measurement of n_N by VUVAS. The relatively large error bars were caused by the fact that n_N was obtained from weak absorption less than 10% in the present experimental condition. The vertical error bars represent the ambiguity in the linear fitting for the relationship between the QMS signal and the flow rate of ammonia added for the calibration. The dotted line indicates $S_{NH_3} = \Gamma_N A_N$, which means the conservation of nitrogen atoms. As shown in Fig. 4, the majority of the plot points coincide with $S_{NH_3} = \Gamma_N A_N$.

Figure 5 shows the correlation between the synthesis rate of ammonia and the integrated flux of atomic hydrogen. The integrated flux of atomic hydrogen was estimated by the same manner as that for atomic nitrogen with $L_H = 14$ cm. The dotted line indicates $S_{NH_3} = \frac{1}{3}\Gamma_H A_H$, which represents the conservation of hydrogen atoms. As shown in Fig. 5, all the plot points locate below $S_{NH_3} = \frac{1}{3}\Gamma_H A_H$, and we observed the remarkable saturation of S_{NH_3} with $\Gamma_H A_H$.

Figure 6 shows the relationship between the synthesis rate of ammonia and the integrated flux of molecular nitrogen at vibrational excited states ($v \geq 1$). The integrated flux was estimated by the same manner as that for atomic nitrogen and atomic hydrogen, where we needed the estimation of the transport length of vibrational excited molecular nitrogen. However, we had no data on the lifetime of vibrational excited molecular nitrogen. We assume in this work

that the effective surface area, where vibrational excited molecular nitrogen can work for the synthesis of ammonia, is equal to that of atomic hydrogen. This is because, the lifetime of vibrational excited molecular nitrogen is expected to be long enough according to the work by Black *et al.*,[19] but vibrational excited molecular nitrogen cannot work for the synthesis of ammonia without the help of atomic hydrogen. As shown in Fig. 6, the integrated flux of vibrational excited molecular nitrogen was three orders of magnitude higher than the synthesis rate of ammonia. No clear correlation was found between the synthesis rate of ammonia and the integrated flux of vibrational excited molecular nitrogen.

3.4 Important species for ammonia synthesis

Atomic nitrogen, atomic hydrogen, and vibrational excited molecular nitrogen are transported to the surface of the stainless-steel vacuum chamber simultaneously, and all of them could contribute to the synthesis of ammonia. The objective of the present work is to identify the most important species in the ammonia synthesis, based on the correlation between the synthesis rate and the integrated fluxes of the three active species. The experimental result shown in Fig. 4 clearly indicates that the synthesis rate of ammonia is dominated by the adsorption flux of atomic nitrogen on the surface of the stainless-steel tube. In addition, according to the fact that the majority of the plot points coincide with $S_{NH_3} = \Gamma_N A_N$, the adsorption probability of atomic nitrogen is estimated to be close to unity, and almost all nitrogen atoms transported to the surface of the stainless-steel tube are used for the synthesis of ammonia. The adsorption probability close to unity is greater than the surface loss probability evaluated from Fig. 2 ($\alpha_N \sim 0.2$), but the difference may be related to the fact that $\alpha_N \sim 0.2$ was evaluated from the lifetime of atomic nitrogen in the afterglow phase. The experimental result shown in Fig. 5 also suggests that the synthesis rate of ammonia is governed by adsorption of atomic nitrogen, and there is a surplus of hydrogen atoms in the present experimental condition. The surplus of hydrogen atoms is owing to the fact that the flux of atomic hydrogen is greater than the flux of atomic nitrogen more than three times. The surplus of atomic hydrogen is also seen in the late afterglow of the pulsed discharge after the disappearance of atomic nitrogen (Fig. 3(a)). The higher flux of atomic hydrogen may be a general situation that is realized in other plasma sources. This is because, the degree of dissociation of molecular hydrogen in plasmas is usually higher than that of molecular nitrogen,[15,30–33] and the thermal mean velocity of atomic hydrogen is faster than that of atomic nitrogen. The synthesis rate of ammonia would possibly be dominated by the flux of atomic hydrogen, if the plasma is produced using nitrogen-hydrogen mixture with $P_{N2}/P_{H2} \gg 1$.

The experimental result shown in Fig. 6 indicates the negligible contribution of vibrational excited molecular nitrogen to the ammonia synthesis. It is widely understood that atomic nitrogen has a higher adsorption probability than molecular nitrogen since it is a radical with unpaired electron. On the other hand, some authors report the enhanced dissociative adsorption probability of molecular nitrogen if it is excited vibrationally.[34–36] Since the vibrational temperature of molecular species in a plasma is higher than the translational temperature, it is argued that the origin of activated reactions in plasma-assisted catalytic synthesis of ammonia is the vibrational excitation. In a recent publication, we reported the positive correlation between the flux of vibrational excited molecular nitrogen and the synthesis rate of ammonia, when a ruthenium catalyst was irradiated with the spatial afterglow of an atmospheric-pressure nitrogen plasma.[13] A point was that the flux of vibrational excited molecular nitrogen was more than four orders of magnitude higher than that of atomic nitrogen in the experiment using the atmospheric-pressure plasma. Figure 7 shows the comparison among the averages of the integrated flux of atomic nitrogen, the integrated flux of vibrational excited molecular nitrogen, and the synthesis rate of ammonia in the present experimental condition. The error bars show the ranges of the present experimental results. As shown in the figure, the integrated flux of atomic nitrogen is higher than 10^{-3} times the flux of vibrational excited molecular nitrogen. This is an important difference from the previous experiment using the atmospheric-pressure plasma.

A paper by Bayer *et al.* reports the dominant contribution of atomic nitrogen to the ammonia synthesis using a radio-frequency-driven atmospheric-pressure plasma.[37] In their discharge, the density of vibrational excited molecular nitrogen is hundred times higher than that of atomic nitrogen. The flux ratio between atomic nitrogen and vibrational excited molecular nitrogen in the present experiment is rather close to that in the experiment by Bayer *et al.*, even though a low-pressure plasma source is used in the present experiment. Thus, the dominant contribution of atomic nitrogen is the common conclusion of the two experiments with similar composition ratios of atomic nitrogen and vibrational excited molecular nitrogen. Our previous work[13] suggests that the surface adsorption probability of vibrational excited molecular nitrogen is higher than 10^{-5}, while the present work suggests that it is lower than 10^{-3}. Note that these adsorption probabilities are evaluated based on the density of $N_2(v \geq 1)$, and they are rough estimation without considering the vibrational distribution. The adsorption probability of molecular nitrogen may be sensitive to the vibrational quantum number,[38] and a higher vibrational state may have a higher adsorption probability. The adsorption probability must be examined as a function of the vibrational quantum number in a future work.

4. Conclusions

In this work, we examined the correlation between the synthesis rate of ammonia and the fluxes of atomic nitrogen, atomic hydrogen, and molecular nitrogen at vibrational excited states in low-pressure nitrogen-hydrogen mixture plasmas. It was found that the integrated flux of atomic nitrogen roughly coincided with the synthesis rate of ammonia, indicating that almost all nitrogen atoms transported to the surface of the stainless-steel tube are used for the synthesis of ammonia. On the other hand, the synthesis rate was saturated with the flux of atomic hydrogen, and there was a surplus of hydrogen atoms in the present experimental condition. We observed no correlation between the synthesis rate and the flux of vibrational excited molecular nitrogen. The experimental results indicate that the adsorption of atomic nitrogen was the rate limiting step in the synthesis process of ammonia in the present experimental condition, where the flux of atomic nitrogen was 10^3 times lower than the flux of vibrational excited molecular nitrogen.

Acknowledgments

This work was supported by JST CREST JPMJCR19R3, JST A-STEP JPMJSF23C1, and JSPS KAKENHI 23H01163.

References

1) A. Klerke, C. H. Christensen, J. K. Nørskov, and T. Vegge, J. Mater. Chem. **18**, 2304 (2008).
2) R. Lan R, J. T. S. Irvine, and S. Tao, Int. J. Hydrogen Energ. **37**, 1482 (2012).
3) C. Smith, A. K. Hill, and L. Torrente-Murciano, Energy Environ. Sci. **13**, 331 (2020).
4) M. Wang, M. A. Khan, I. Mohsin, J. Wicks, A. H. Ip, K. Z. Sumon, C.-T. Dinh, E. H. Sargent, I. D. Gates, and M. G. Kibria, Energy Environ. Sci. **14**, 2535 (2021).
5) C. A. Fernandez and M. C. Hatzell, J. Electrochem. Soc. **167**, 143504 (2020).
6) G. Qing, R. Ghazfar, S. T. Jackowski, F. Habibzadeh, M. M. Ashtiani, C.-P. Chen, M. R. Smith III, and T. W. Hamann, Chem. Rev. **120**, 5437 (2020).
7) J. Hong, S. Prawer, and A. B. Murphy, ACS Sustainable Chem. Eng. **6**, 15 (2018).
8) J. Shah, W. Wang, A. Bogaerts, and M. J. Carreon, ACS Appl. Energy Mater. **1**, 4824 (2018).
9) K. H. R. Rouwenhorst, H. G. B. Burbach, D. W. Vogel, J. N. Paulí, B. Geerdink, and L. Lefferts, Catal. Sci. Technol. **11**, 2834 (2021).
10) M. Kitano, S. Kanbara, Y. Inoue, N. Kuganathan, P. V. Sushko, T. Yokoyama, M. Hara, and H. Hosono, Nat. Commun. **6**, 6731 (2015).
11) P. Mehta, P. Barboun, F. A. Herrera, J. Kim, P. Rumbach, D. B. Go, J. C. Hicks, and W. F. Schneider, Nat. Catal. **1**, 269 (2018).
12) Y. Engelmann, K. van't Veer, Y. Gorbanev, E. C. Neyts, W. F. Schneider, and A. Bogaerts, ACS Sustain. Chem. Eng. **9**, 13151 (2021).
13) A. Miyake, N. Shirai, and K. Sasaki, J. Appl. Phys. **135**, 213301 (2024).
14) K. Sasaki, Y. Kawai, and K. Kadota, Rev. Sci. Instrum. **70**, 76 (1999).
15) Y. Horikawa, K. Kurihara, and K. Sasaki, Jpn. J. Appl. Phys. **49**, 026101 (2010).
16) A. G. Mitchell and M. W. Zemansky, "Resonance Radiation and Excited Atoms," (Cambridge University Press, Cambridge, England, 1961).
17) J. Jiang, C. Richards, I. Adamovich, and P. J. Bruggeman, Plasma Sources Sci. Technol. **31**, 0LT03 (2022).
18) S. Hosoyama, M. Yamazaki, and K. Sasaki, Plasma Fusion Res. **17**, 1406070 (2022).
19) G. Black, H. Wise, S. Schechter, and R. L. Sharpless, J. Chem. Phys. **60**, 3526 (1974).
20) J. Takahashi and K. Sasaki, Contrib. Plasma Phys. **64**, e202300167 (2024).
21) P. J. Chantry, J. Appl. Phys. **62**, 1141 (1987).
22) J. E. Morgan and H. I. Schiff, Can. J. Chem. **42**, 2300 (1964).

23) G. Cernogora and N. Sadeghi, Chem. Phys. Lett. **74**, 417 (1980).
24) G. Blyth, A. A. Clifford, P. Gray, and J. I. Waddicor, J. Chem. Soc., Faraday Trans 1 **83**, 751 (1987).
25) S. F. Adams and T. A. Miller, Plasma Sources Sci. Technol. **9**, 248 (2000).
26) H. Singh, J. W. Coburn, and D. B. Graves, J. Appl. Phys. **88**, 3748 (2000).
27) W. M. M. Kessels, F. J. H. van Assche, J. Hong, D. C. Schram, and M. C. M. van de Sanden, J. Vac. Sci. Technol. A **22**, 96 (2004).
28) S. Takashima, K. Takeda, S. Kato, M. Hiramatsu, and M. Hori, Jpn. J. Appl. Phys. **49**, 076101 (2010).
29) D. Marinov, O. Guaitella, T. de los Arcos, A. von Keudell, and A. Rousseau, J. Phys. D: Appl. Phys. **47**, 475204 (2014).
30) E. Es-sebbar, Y. Benilan, A. Jolly, and M.-C. Gazeau, J. Phys. D: Appl. Phys. **42**, 135206 (2009).
31) S. Takashima, S. Arai, M. Hori, T. Goto, A, Kono, M. Ito, and K. Yoneda, J. Vac. Sci. Technol. A **19**, 599 (2001).
32) S. Takashima, M. Hori, T. Goto, A. Kono, M. Ito, and K. Yoneda, Appl. Phys. Lett. **75**, 3929 (1999).
33) J. Jolly and J.-P. Booth, J. Appl. Phys. **97**, 103305 (2005).
34) L. Romm, G. Katz, R. Kosloff, and M. Asscher, J. Phys. Chem. B **101**, 2213 (1997).
35) L. Diekhöner, H. Mortensen, A. Baurichter, E. Jensen, V. V. Petrunin, and A. C. Luntz, J. Chem. Phys. **115**, 9028 (2001).
36) K. H. R. Rouwenhorst and L. Lefferts, J. Phys. D: Appl. Phys. **54**, 393002 (2021).
37) B. N. Bayer, P. J. Bruggeman, and A. Bhan, ACS Catal. **13**, 2619 (2023).
38) B. N. Bayer, S. Raskar, I. V. Adamovich, P. J. Bruggeman, and A. Bhan, Plasma Sources Sci. Technol. **32**, 125005 (2023).

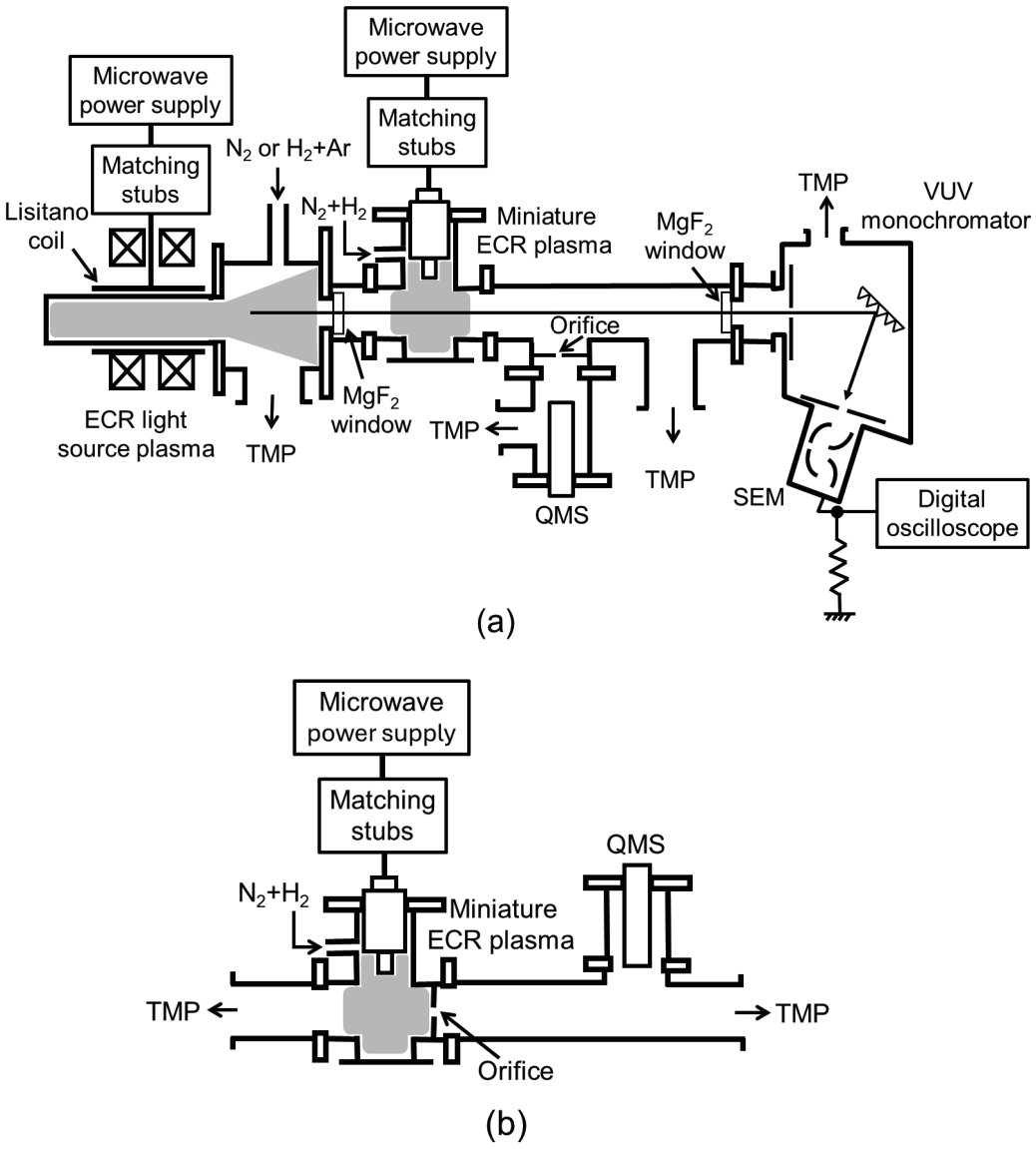

Fig. 1. Schematic illustrations of experimental apparatus. (a) System for measuring the densities of atomic nitrogen and atomic hydrogen by VUVAS. The synthesis rate of ammonia was measured simultaneously using calibrated QMS. (b) System for measuring the density of molecular nitrogen at vibrational excited states by threshold ionization mass spectrometry. The synthesis rate of ammonia was also measured using same QMS as that used for threshold ionization mass spectrometry.

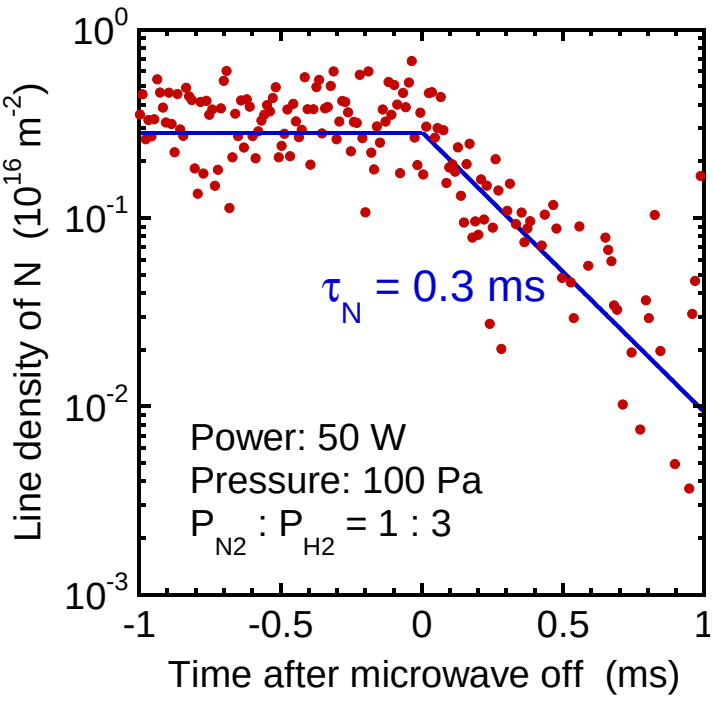

Fig. 2. Temporal variation of the line-integrated density of atomic nitrogen in the afterglow of a pulsed discharge.

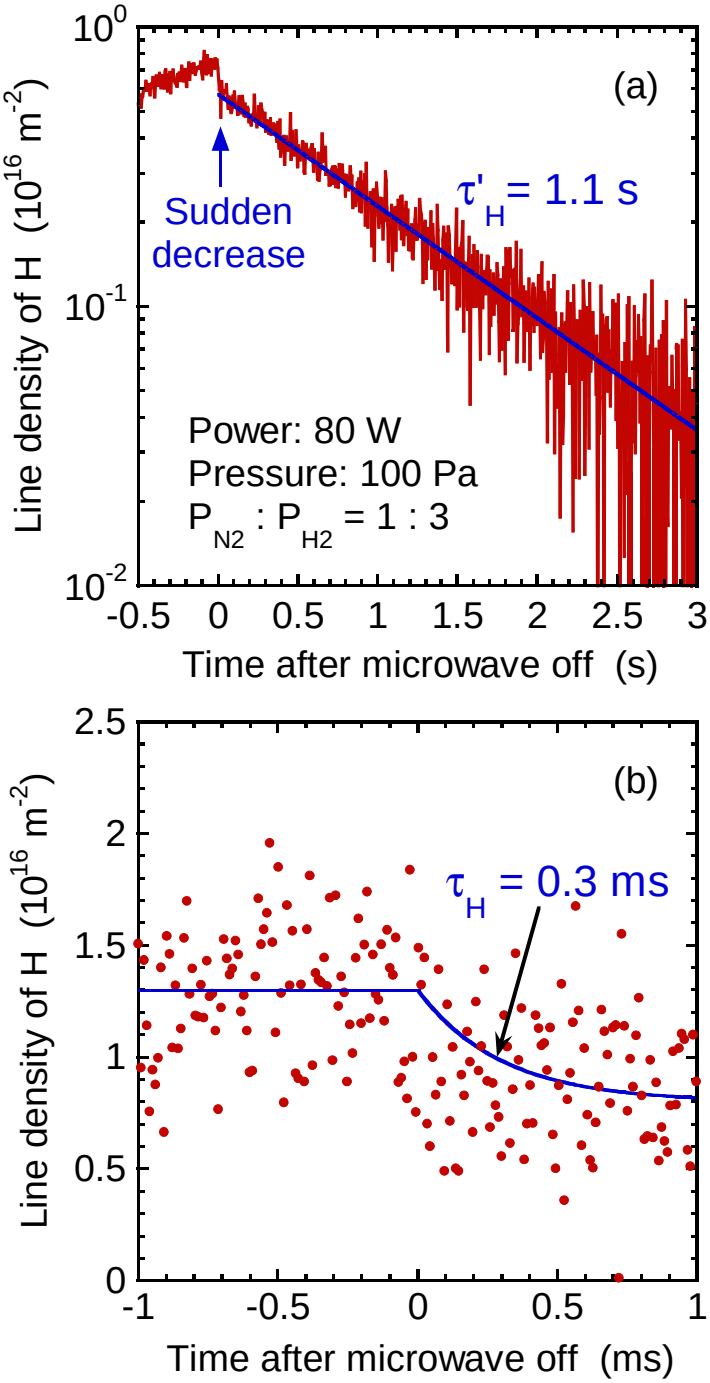

Fig. 3. Temporal variations of the line-integrated density of atomic hydrogen in the afterglow of pulsed discharges. (a) shows the entire decay of the atomic hydrogen density, and (b) shows the decay of the atomic hydrogen density immediately after the termination of the microwave power.

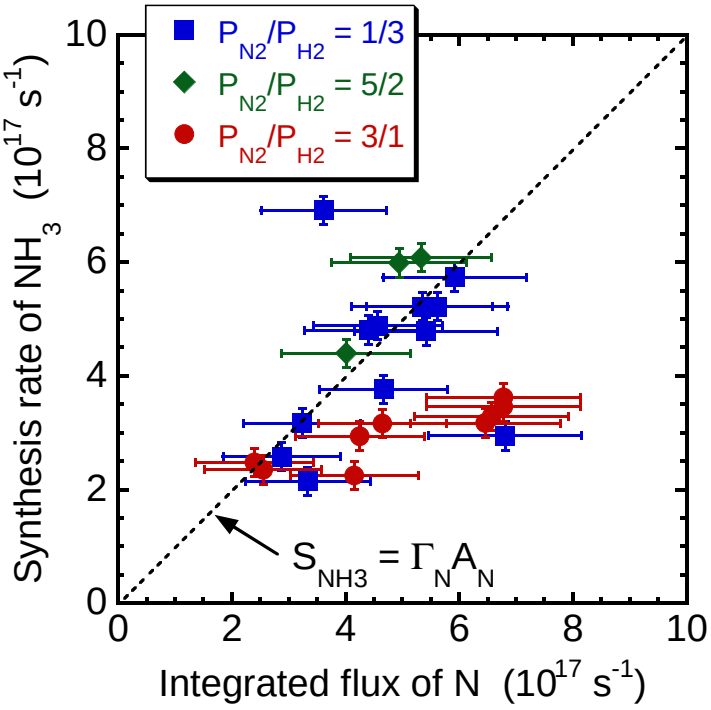

Fig. 4. Correlation between the synthesis rate of ammonia S_{NH_3} and the integrated flux of atomic nitrogen $\Gamma_N A_N$. The dotted line shows the relationship $S_{NH_3} = \Gamma_N A_N$.

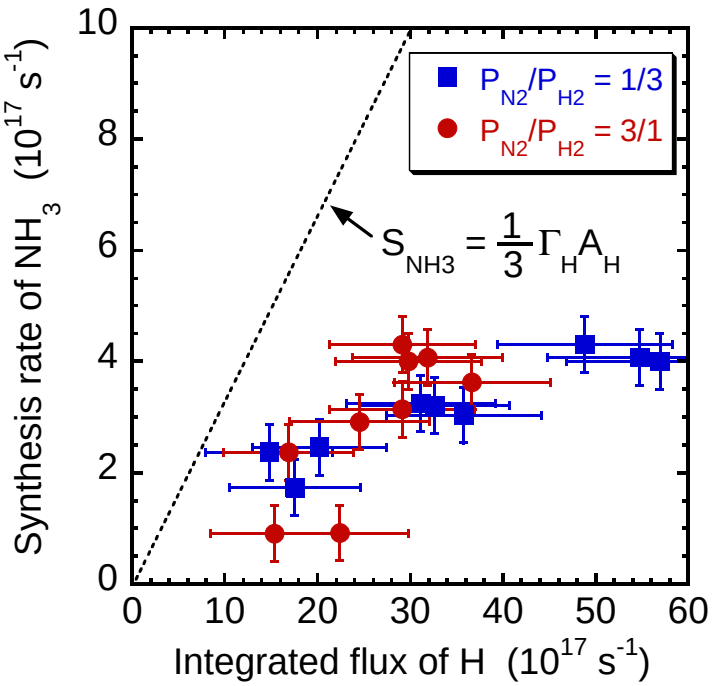

Fig. 5. Correlation between the synthesis rate of ammonia S_{NH_3} and the integrated flux of atomic hydrogen $\Gamma_H A_H$. The dotted line shows the relationship $S_{NH_3} = \frac{1}{3}\Gamma_H A_H$.

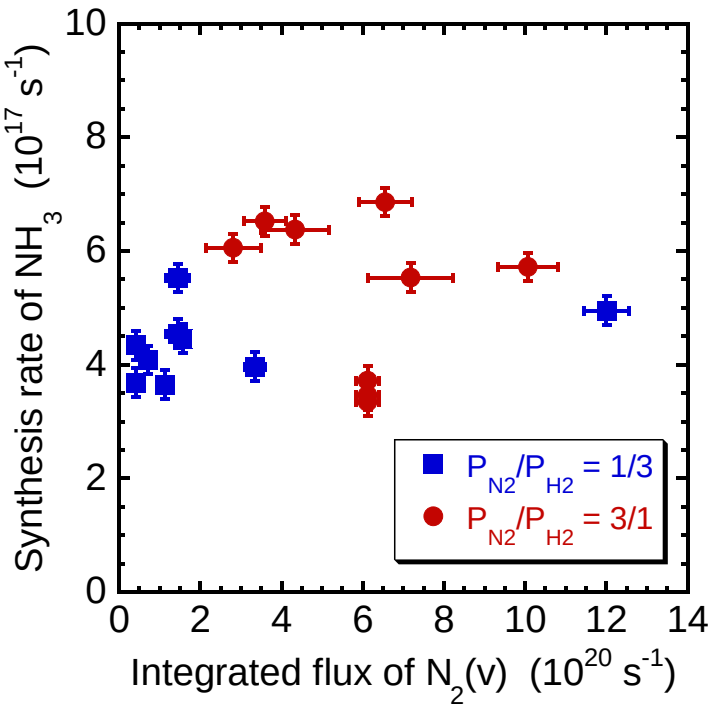

Fig. 6. Relationship between the synthesis rate of ammonia and the integrated flux of vibrational excited molecular nitrogen.

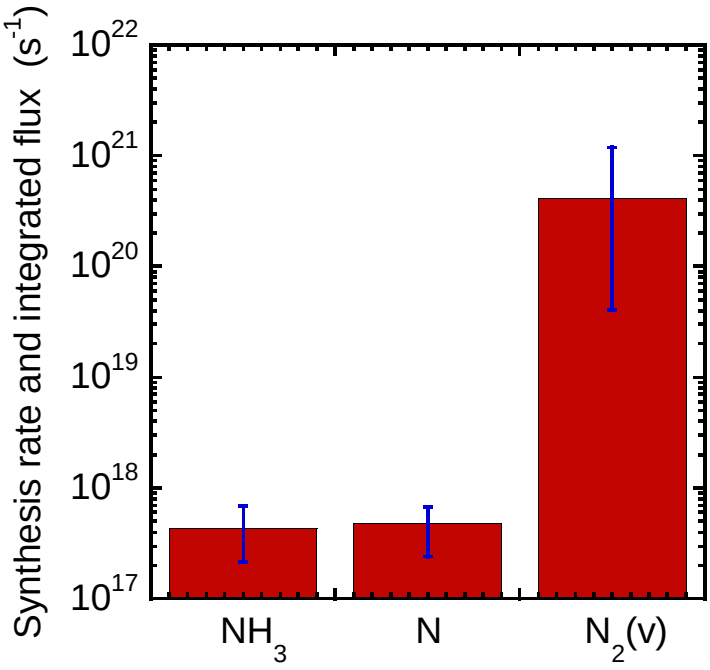

Fig. 7. Comparison among the synthesis rate of ammonia, the integrated flux of atomic nitrogen, and the integrated flux of vibrational excited molecular nitrogen.